

Article

The Effects of Hydraulic Jumps Instability on a Natural River Confluence: The Case Study of the Chiaravagna River (Italy)

Annalisa De Leo ^{1,*} , Alessia Ruffini ^{1,2} , Matteo Postacchini ² , Marco Colombini ¹ 
and Alessandro Stocchino ¹ 

¹ Università degli Studi di Genova, DICCA, via Montallegro 1, 16145 Genova, Italy; alessia.ruffini@outlook.it (A.R.); col@dicca.unige.it (M.C.); alessandro.stocchino@unige.it (A.S.)

² Università Politecnica delle Marche, DICEA, via Brecce Bianche 12, 60131 Ancona, Italy; m.postacchini@staff.univpm.it

* Correspondence: annalisa.deleo@edu.unige.it

Received: 29 May 2020; Accepted: 13 July 2020; Published: 16 July 2020



Abstract: The occurrence and the effects of hydraulic jump instabilities on a natural river confluence in a small river basin in Liguria (Italy) is here investigated. Hydraulic jump instability has been extensively studied in controlled and simplified laboratory rectangular flumes. In the present study, a scaled physical model of the Chiaravagna River and Ruscarolo Creek confluence has been used, retaining the realistic geometry of the reaches. This reach has been subject to frequent floods in the last twenty years and the entire area of the confluence has been redesigned to decrease the flood risk. A series of experiments has been performed varying the discharge on the two reaches and the geometrical configurations. Free surface levels and two dimensional horizontal velocities have been measured in several positions along the physical model. The analysis of the water levels and velocities reveals that oscillations characterised by large amplitude and low frequency occur under particular hydraulic conditions. These oscillations have been found to be triggered by the hydraulic jump toe instability of the smallest reach of the confluence. Aiming at reducing the amplitude of the oscillations, which can be of the order of the flow depth, possible constructive solutions have been tested to control or damp the oscillations. Indeed, the insertion of a longitudinal dyke at the confluence has proven to be an effective solution to limit the amplitude of the transversal oscillations.

Keywords: river confluence; hydraulic toe jump instability; flood risk

1. Introduction

Hydraulic jumps are common phenomena in free surface flows in natural rivers, artificial canals and industrial applications. They occur whenever a supercritical high velocity flow impacts a subcritical low-velocity flow and the abrupt transition leads to a strong energy dissipation. The role of the jumps in hydraulics [1] and environmental engineering [2–4] is well known and this motivated a great number of scientific contributions. Starting from the seminal studies of Bakhmeteff [5] and Rouse and Siao [6], a considerable effort has been devoted to understand the complex turbulent flow involved, the prediction of the free surface profile and its stability. Applying the integral form of the conservation of momentum, it is found that the momentum of the supercritical flow balances the momentum of the subcritical one downstream in correspondence of the hydraulic jump. In the case of a prismatic rectangular channel, neglecting the flow resistance and velocity distribution effects, the balance provides the classical Bélanger relationship between the flow depth upstream (d_1) and

downstream (d_2) of the hydraulic jump itself as a function of the inflow Froude number (Fr_1), defined as $Fr_1 = V_1 / \sqrt{gd_1}$, which reads [7–9]:

$$\frac{d_2}{d_1} = \frac{1}{2}(\sqrt{1 + 8Fr_1^2} - 1) \quad (1)$$

Chanson (2012) [10] extended the Bélanger equation to a generic cross-section with the inclusion of flow resistance. Starting from this analytical description, many studies have concentrated on the turbulent characteristics of the hydraulic jumps that are very often complicated by a strong aeration of the flow [11–18]. Most of the cited works were based on experimental analysis. However, the numerical computation of river flow, including a detailed representation of the hydraulic jumps, has been subject to an analogous large number of studies, see among others [19–22] and references herein.

As seen in Mossa (1999) and Wang and Chanson (2015), different kinds of hydraulic jumps might occur. The present work is mostly interested in investigating the hydraulic jump toe instability (here and after indicated as jump instability). Indeed, the high intensity turbulent flow that characterises these phenomena and the air–water interactions often lead to free-surface instabilities and/or the hydraulic jump toe oscillations, see among others [12,15–17,23–25]. In particular, Murzyn and Chanson (2009) and Wang and Chanson (2015) focused on how the Strouhal number $S_t = F_{toe}d_1/V_1$ varies with respect to the Reynolds number $Re = V_1d_1/\nu$, where the former characterises the oscillating nature of a physical system and the latter the ratio between inertial and viscous stresses. Moreover, F_{toe} is the hydraulic jump toe frequency of oscillation deduced from a spectral analysis of the displacement of the toe itself, d_1 and V_1 are the flow depth and velocity upstream the toe and ν the water kinematic viscosity. Both the aforementioned contributions remark out that for relatively low Reynolds numbers, the Strouhal number remains nearly constant, whereas Wang and Chanson (2015) also explored the range of high Reynolds numbers showing that the Strouhal number increases and that the rapid jump toe oscillations are owed to air entrapment at the impact point (see also Long et al. (1991)). Other studies, e.g., conducted by Zhang et al. (2013), performed a comparison between S_t and Re , and established a relation between them. Mossa and Tolve (1998), instead, highlighted that it is possible to recognise the oscillating nature of the jump toe position through the use of the Fast Fourier Transform (FFT) technique, whereby a quasi-periodic oscillation of both the jump toe and the free surface implies the presence of a neat peak in the spectrum. The same technique has been used by Kramer and Valero (2020). They performed a spectral analysis on velocity signals collected by optical flow measurements, with the aim to incorporate the aerated nature of the hydraulic jump.

All the above contributions were based on experimental studies performed in laboratory rectangular flumes. A theoretical model explaining the onset of the instability is still lacking. It is reasonable to assume that the inflection point in the mean velocity profile at the hydraulic jump toe represents a sufficient condition for an inviscid instability [26]. However, to our knowledge no specific studies are available in the literature. Following the experimental approach used in the cited works, the present study focuses on the possibility that this kind of instabilities could arise also in more complex geometries and tries to assess their implications on the flood risk in natural rivers. In particular, the area of interest is the confluence between the Chiaravagna River and the Ruscarolo Creek, a natural river confluence on which several floods occurred in the past twenty years.

Rivers with small catchment areas, less than 50 km², are subject to the occurrence of the so called flash floods: short and intense events owed to extreme rainfalls that causes a quick response of the river reach.

In this context, the confluence between the Chiaravagna River and the Ruscarolo Creek has been subject to recent river-works in order to reduce the flooding risks. The design solution has been investigated using a scaled laboratory model and tested for the design flow discharge, which is chosen as the event with 200 years return period. The experiments showed the occurrence of intense free surface oscillations just downstream of the river confluence. The amplitude of the oscillations was almost comparable with the mean depth, thus, reducing the positive effect of the

design configuration in terms of flood risk. The main cause of the free surface oscillations is rooted in an instability mechanism similar to the hydraulic jump toe instability discussed in the above mentioned contributions. The high flow coming from the Ruscarolo Creek generated an oblique hydraulic jump, which was found to be unstable under certain flow discharge conditions and the resulting toe oscillation frequency was close to the transversal free mode of oscillation of the free surface downstream the confluence. The understanding of this mechanism suggested some modification of the originally designed configuration in order to limit the effect of the hydraulic jump instability.

The paper proceeds with Section 2.1, regarding the description of the study area, then the physical model, measuring techniques and data analysis are described in the rest of Section 2. Section 3 describes the results of the experiments performed on the different geometrical and hydrological conditions, followed by a discussion. Eventually, the conclusions are drawn in Section 5.

2. Materials and Methods

2.1. Study Area

The basin of the Chiaravagna River is placed on the Tyrrhenian side of the Ligurian Apennines, close to Genova Sestri Ponente, as shown in Figure 1. It is characterised by a narrow and elongated shape and it extends over an area of about 11 km². The main reach is only 3.3 km long and it is characterised by limited ramifications with the exception of the Ruscarolo Creek; downstream the confluence it flows towards the airport of Genova, on the west side of the Polcevera River. Along its entire flow, the Chiaravagna River presents various obstacles: mining activities, the largest landfill in the Region and intense and chaotic urban development. After an intense flooding event that occurred in October 2010, the local Administration decided to start works on the riverbed in order to increase the hydraulic capacity and, thus, to decrease the flooding risk.



Figure 1. Satellite images of the study area and its location on the Italian territory. The red arrow indicates the Chiaravagna River and the orange arrow the Ruscarolo Creek. Image taken from Google map and the web portal of the Liguria Region.

2.2. Physical Model Description

In order to test the designed configuration, a physical scaled model of the confluence of the Chiaravagna River and the Ruscarolo Creek has been prepared in the hydraulic Laboratory of the Department of Civil, Chemical and Environmental Engineering of the University of Genova. The geometric reduction scale, defined as the ratio of the lengths on the prototype (indicated with the P subscript) compared to the lengths on the model (indicated with the M subscript), has been chosen as $\lambda = L_P/L_M = 35$. Scale reproduction of free surface flows is typically achieved through a partial similarity of Froude, defined as $Fr = V/\sqrt{gd}$ where V and d are the average velocity and depth of the current, g the acceleration of gravity, thus accepting that the Reynolds number is not preserved in the model [27]. Once the geometrical reduction scale λ has been set, Froude's similarity determines the scales for other quantities. In particular, fluid velocity, time and volumetric flow rate assume the following reduction scales:

$$\frac{U_P}{U_M} = \lambda^{1/2} = 5.92 \quad \frac{T_P}{T_M} = \lambda^{1/2} = 5.92 \quad \frac{Q_P}{Q_M} = \lambda^{5/2} = 7247 \quad (2)$$

In this case, the correct representation of the flow resistance requires special attention, owing to the reduced value of the Reynolds number on the model. In fact, the model Reynolds number is reduced by about two hundred times compared to the one in the prototype. This implies, for example, that the flow in the physical model might be in the hydrodynamically rough regime, as it typically occurs in real river flows. On the contrary, a smooth flow regime is observed on the model, leading to a conductance coefficient C that depends on the Reynolds number alone and not on the dimensional roughness. In the present case, owing to the geometrical scale adopted and the dimensional roughness of the material used for the model construction, the flow falls in the smooth case and, using the Blasius resistance law valid in this condition, it turns out that the mean non dimensional smooth conductance coefficient of the model $C_M = 17$ corresponds on the prototype (in the rough regime) to a Gauckler–Strickler coefficient of $55 \text{ m}^{1/3}/\text{s}$, which is adequate for a concrete pavement.

Moreover, when dealing with free surface flows, Chanson and Gualtieri (2008) noted that possible air entrapment in hydraulic jumps could not be correctly reproduced under a Froude similarity, owing to the different processes that regulate aeration, i.e., surface tension. Even though this is probably not the main mechanism driving the hydraulic jump instability.

A schematic view of the physical model is shown in Figure 2, where it is clearly visible the part of the model representing the confluence and the hydraulic circuit used to feed the model. In particular, the model represents the following reaches (see Figure 3, for section references):

- two separate inlet channels, about 50 m long at the prototype scale, with a rectangular section with constant width that connects the feeding tanks (separated for Chiaravagna and Ruscarolo) to the actual model (sections 0–15, sections 0–33);
- a reach of about 60 m of the Chiaravagna River upstream of the confluence and including the via Giotto bridge and two weirs (sections 15–13.5);
- a reach of about 60 m of the Ruscarolo Creek upstream of the confluence and including the via Giotto bridge, the arched stone footbridge and a weir (section 31–30.1);
- a reach of about 70 m where the confluence insists, which includes the crossing of Via Manara, the reach below the ELSAG building cover, divided in three barrel-vaults, and a weir downstream of the building itself (sections from 13.5 and 30.1 to 12);
- a final reach of about 65 m downstream the ELSAG building where a car park area is located on the left bank (sections 12–11).

The Chiaravagna and Ruscarolo branches of the model have been fed with two separate piping starting from a common tank, placed on the ground floor of the laboratory. The flowing discharges are regulated through two butterfly valves manually operated. Moreover, in Figure 3, some other features are reported: in red and white are shown the underpinning walls (see the Figure S1 in the

Supplementary Materials), in brown the sewage box (Figures S1, S2 and S3) and in filled black the ELSAG building’ pillars (painted in yellow and blue in Figures S4 and S5) above which Via Manara, the building itself and a pedestrian bridge are placed. All the superstructures are represented with dashed lines: proceeding left to right, Via Giotto insists both on the Chiaravagna and Ruscarolo reaches without any obstacles on the flow (i.e., pillars), then, on the Ruscarolo Creek, an old pedestrian arch bridge is present (see Figure S6) and then, as already mentioned, Via Manara, ELSAG building and the pedestrian bridge. The black transversal element (Figure 4 and Figure S7 in the Supplementary Materials), are the supporting beams of the ELSAG Building. Weirs can be found between Section 14.85 and 14.80, and Section 14 and 13.5 (see Figure S8), Section 30.1 and 29 and Section 12 and 11.9, respectively shown in Figures S9 and S5 (see Figure 3 for section references). Between Section 11.2 and 11, a car park has been built on the left bank of the reach. It leans on eight pillars placed directly on the riverbed (see Figure S10). In the bottom panel of Figure 3, there are three different position of a dyke: in Figure S11 position B is shown.

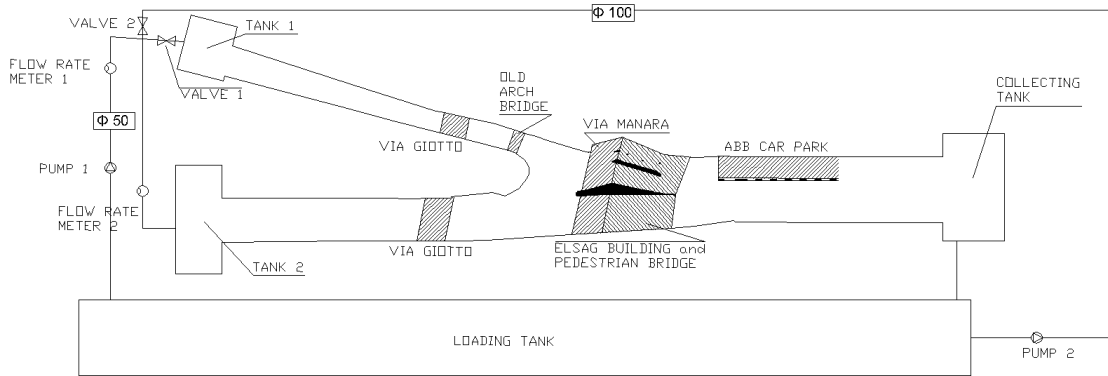


Figure 2. Plan view of the physical model.

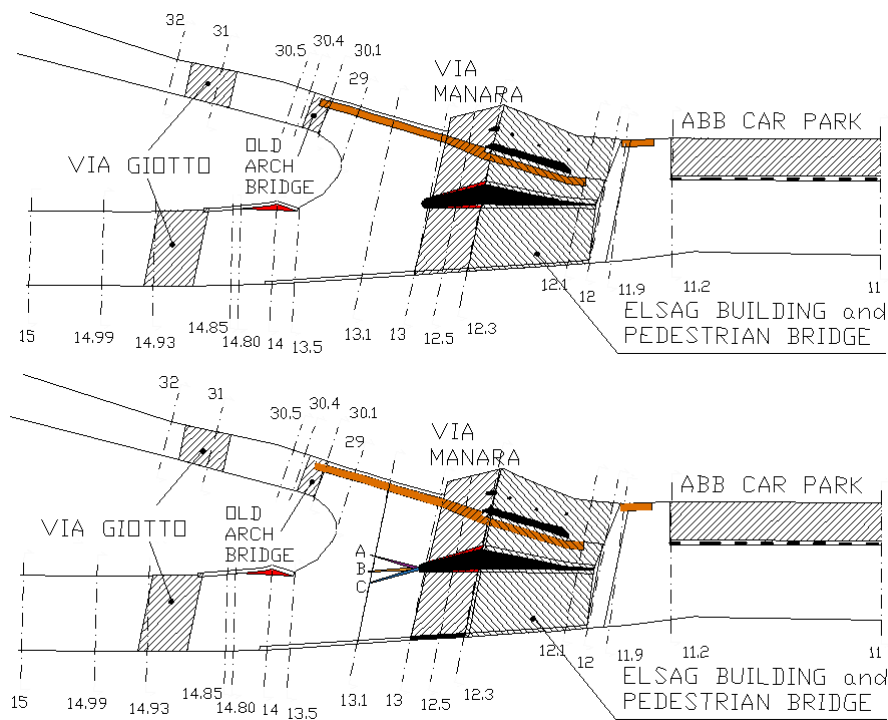


Figure 3. Plan view of the geometrical configurations tested. Top panel: original project; Bottom panel: configuration with three position of the longitudinal dyke.

2.2.1. Measuring Techniques and Data Analysis

The physical model has been equipped with several measuring instruments. In particular, the flow discharge has been monitored using two electromagnetic flowmeters PROMAG P, one on each feeding pipeline. During each experiment, the water level and the velocities in different position of the model were recorded. In order to perform the water level measurements, an ultrasound gauge (Honeywell model 946-A4V-2D-2C0-380E, with 30 cm range and an accuracy of 0.2% of the full scale) has been used. The velocities have been recorded through a micropropeller (velocity range 0–1.2 m/s) and an acoustic velocimeter (Nortek Vectrino ADV probe with a velocity range ± 0.01 –4 m/s and an accuracy $\pm 0.5\%$ of measured value ± 1 mm/s). All the instruments have been installed on a movable carrier: this allowed to place the instruments on several and repeatable positions. In Figure 4 the measuring point of the water level (panel c) and the velocity (panel a) are shown. Note that in the latter, all the velocity measuring points are represented. Indeed, a complete map of the velocity has been obtained only in few runs, owed to the complexity of these measurements in an unsteady situation, as the one here examined. In the following, most of the discussion of the velocity spectra is focused on signals measured in few stations along a single cross section located in the confluence area. Moreover, not all features of the model are here illustrated, e.g., just few ELSAG Building's pillars are shown in black. The water level measuring points have been used to produce longitudinal free surface profiles along several paths indicated in Figure 4b. All instruments have been connected to a DAQ unit (National Instrument model 6250). The ultrasound gauge and the micropropeller have been used with an acquisition frequency of 100 Hz, whereas the acquisition frequency of the acoustic velocimeter was set at 200 Hz. The acquired signals have been analysed in both time and frequency domains. In particular, probability density function and its moments have been calculated for each signal, providing estimates of its mean and standard deviation values. In the frequency domain, a spectral analysis has been performed, by computing the power spectral density (PSD) estimate of the longitudinal velocity v_x ($S_{v_x}(f)$) and, when appropriate, of the transversal velocity v_y ($S_{v_y}(f)$), using Welch's overlapped segment averaging estimator. The signals are divided into the longest possible segments to obtain as close to but not exceeding 8 segments with 50% overlap. Each segment is windowed with a Hamming window. The modified periodograms are averaged to obtain the PSD estimate.

2.2.2. Experimental Conditions

In the present study, a total of 28 runs have been performed, varying the volumetric discharge and the geometrical configuration of the model. In Table 1, the controlling parameters, i.e., the flow rates, the water depth of the Chiaravagna and Ruscarolo Creek and the corresponding Froude numbers are reported. In the final column, it is indicated whether free surface oscillations were observed during the runs.

To investigate the response of the model in its original design (see Figure 3 top panel), a first set of experiments were performed in different hydraulic scenarios, labelled *1C* and *1R*. In fact, the discharge downstream the confluence was set to the value corresponding to a return period of 200 years. Two combinations of discharges on the upstream reaches producing the same output discharge were tested, one assuming a 200 return time event on the Chiaravagna river and setting the discharge on the Ruscarolo by difference (*1C*), the other assuming a bicentennial event on the Ruscarolo and setting the discharge on the Chiaravagna by difference (*1R*). The experiment *2R* has been performed with the same hydraulic condition of experiment *1R*, but with the insertion of a longitudinal dyke. The experiments labelled *A*, *B* and *C* have been performed with the hydraulic condition of experiment *2R* with the aim to test the dyke orientation that better damp the free surface oscillations associated with the toe jump instability. In particular, the longitudinal dyke, tested in the physical model, consists of wall of height equal to 6 cm, with a rounded tip triangular base of 2 cm width and 32.5 cm length, positioned upstream of the main beam of the ELSAG building (see Figure 3 bottom panel).

The series of experimental runs, labelled from 1 to 23, has been performed with the specific aim to find the critical conditions for the onset of instability. The procedure required to progressively

increase the flow discharges starting from very low values. The experiments have been performed keeping the discharge ratio Q_{ru}/Q_{ch} constant and equal to 26%, i.e., the same hydraulic condition of experiment 1C, in which the maximum discharge is set on the Chiaravagna River. For each run the following quantities have been measured: the discharges in the two branches, the water levels upstream the confluence, both in the Ruscarolo Creek and in the Chiaravagna River, and the relative Froude numbers. Moreover, the velocity at three different locations has been recorded. The locations have been selected along the cross section of the river confluence, namely positions 19, 22 and 25 in Figure 4a, respectively in front of the Chiaravagna River, in the middle of the confluence and in front of the Ruscarolo Creek.

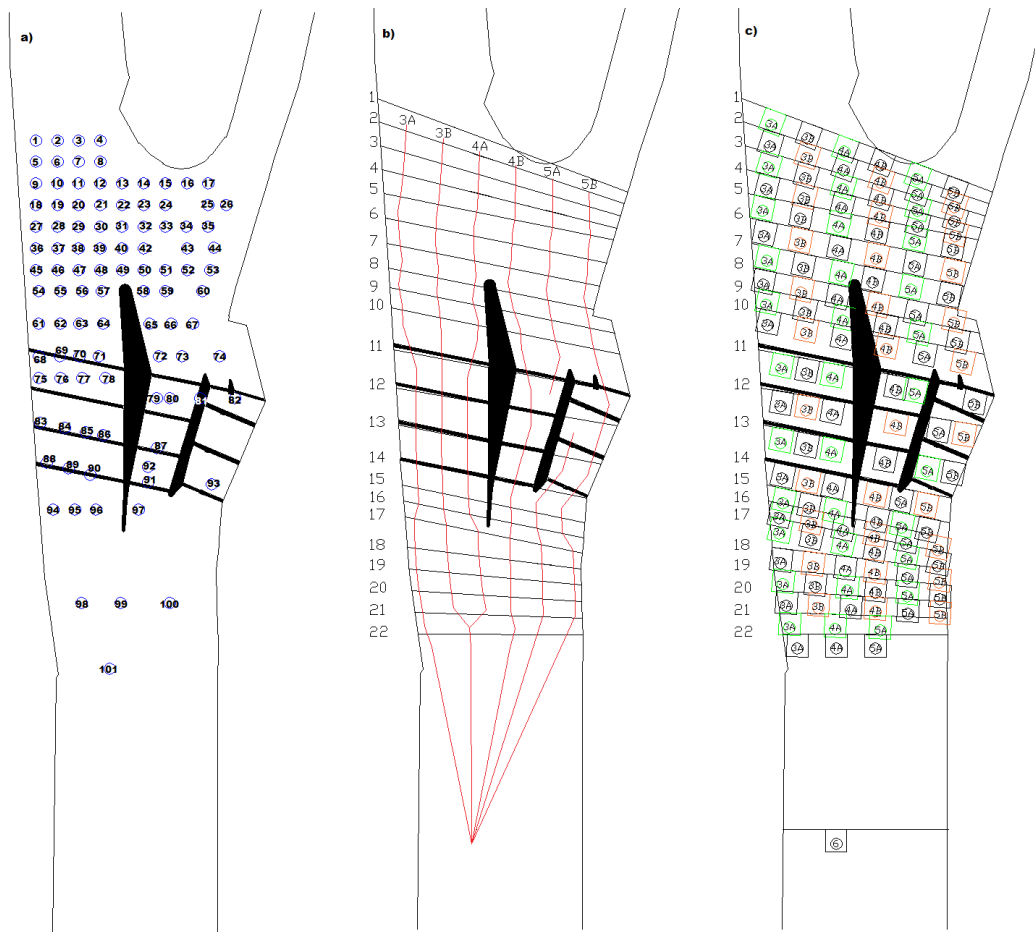


Figure 4. Schematic map of the measurement positions: (a) velocity measurements; (b) longitudinal profiles; (c) free surface level measurements.

Table 1. Experimental parameters of series 2.

RUN n.	Q_{ch} (l/s)	Q_{ru} (l/s)	Q_{ru}/Q_{ch} (l/s)	Q_t (l/s)	Y_{ch} (m)	Y_{ru} (m)	Fr_{ch}	Fr_{ru}	Stability
1C	28.15	7.32	0.26	35.47	0.0427	0.0220	1.8349	2.49	unstable
1R	24.98	10.48	0.42	35.47	0.0367	0.0250	2.04	2.95	unstable
2R	24.98	10.48	0.42	35.47	0.0381	0.0250	1.93	2.95	unstable
A	24.98	10.48	0.42	35.47	0.0380	0.0250	1.94	2.95	unstable
B	24.98	10.48	0.42	35.47	0.0380	0.0250	1.94	2.95	unstable
C	24.98	10.48	0.42	35.47	0.0380	0.0250	1.94	2.95	unstable
1	5.93	1.88	0.25	7.43	0.0178	0.0078	1.43	2.42	stable
2	7.93	2.61	0.26	10.00	0.0231	0.0094	1.30	2.54	stable
3	9.58	3.20	0.26	12.11	0.0302	0.0102	1.05	2.74	unstable
4	9.00	2.94	0.26	11.33	0.0274	0.0098	1.14	2.68	unstable
5	8.53	2.74	0.26	10.71	0.0254	0.0093	1.21	2.71	unstable
6	8.20	2.66	0.26	10.32	0.0241	0.0092	1.26	2.65	unstable
7	8.04	2.64	0.26	10.13	0.0235	0.0092	1.28	2.65	unstable
8	7.65	2.50	0.26	9.64	0.0221	0.0091	1.34	2.56	unstable
9	6.48	2.14	0.26	8.17	0.0189	0.0081	1.43	2.58	unstable
10	5.40	1.80	0.26	6.83	0.0171	0.0077	1.39	2.34	stable
11	6.48	2.16	0.26	8.19	0.0189	0.0082	1.43	2.57	stable
12	4.53	1.50	0.26	5.72	0.0163	0.0070	1.25	2.26	stable
13	5.14	1.68	0.26	6.48	0.0165	0.0075	1.39	2.29	stable
14	5.81	1.90	0.26	7.32	0.0170	0.0077	1.51	2.48	stable
15	6.15	2.03	0.26	7.76	0.0178	0.0079	1.49	2.55	stable
16	6.35	2.10	0.26	8.01	0.0183	0.0080	1.47	2.58	stable
17	6.74	2.21	0.26	8.50	0.0195	0.0083	1.42	2.58	stable
18	7.02	2.30	0.26	8.85	0.0200	0.0086	1.43	2.55	stable
19	7.44	2.41	0.26	9.36	0.0210	0.0088	1.40	2.59	stable
20	7.70	2.51	0.26	9.69	0.0216	0.0091	1.39	2.55	stable
21	8.15	2.63	0.26	10.24	0.0229	0.0092	1.35	2.66	unstable
22	8.37	2.72	0.26	10.53	0.0241	0.0093	1.28	2.68	unstable
23	8.66	2.83	0.26	10.91	0.0255	0.0094	1.22	2.74	unstable

3. Results

In this section, we present the main results of the experimental campaign, focusing our attention on the flow depth and velocity measurement performed in several stations along the river reaches. The time averaged values of the water depth have been used to produce longitudinal free surface profiles along paths indicated in Figure 4b. The detailed analysis of the signals in terms of Power Spectral Density functions, that help in the identification of the characteristic frequencies, have been left for the Discussion section (Section 4).

3.1. Free Surface Local Measurements and Longitudinal Profiles for the Design Discharge

We first present the longitudinal free surface profiles that help to provide an overview of the mean water level along the reach under investigation. In particular, Figure 5a,b report the profiles along the longitudinal paths 3B and 4B, in Figure 4b, for their plan-view locations. Profile 3B starts from upstream the confluence in the centre of the Chiaravagna reach and, following the right bank, it ends downstream the main building. The profile 4B, instead, starts from the confluence and goes through the central aperture below the ELSAG building, ending downstream of the latter, as well as the profile 3B. The profiles, reported in Figure 5, refer to three different configurations, namely 1C, 1R, 2R. Together with the mean value of the water level, indicated with solid symbols, the recorded amplitude of the free surface has been indicated with the error bars. The error bars have been estimated as the mean of the measured water levels that exceeded twice the rms of the signal itself. All configurations share some common features in terms of the mean free surface profiles. Indeed, the two currents upstream are supercritical before entering the confluence, with a Froude number considerably larger than 1; in particular, the Froude number of the Ruscarolo Creek has a typical value of 2.5. The mean profiles are characterised by the presence of two strong hydraulic jumps. The first one is an oblique

jump placed just downstream the confluence where the two rivers meet. The fact that the hydraulic jump is oblique is related to the geometry of the confluence. Indeed, the Ruscarolo Creek enters the confluence at an angle of about 30 degrees with respect to the axis of the Chiaravagna River, which is aligned with the stream-wise direction downstream the confluence. Although the noticeable difference in the flow discharges of the two reaches (i.e., the flow discharge of the Ruscarolo is about the 26% or 42% of the one of the Chiaravagna for the configuration *C* and *R*, respectively) the position and the intensity of this hydraulic jump are slightly affected by the discharge ratio. In fact, by inspecting the profiles of Figure 5 it is clear that the profiles labelled 1R-3B and 1R-4B are characterised by higher water levels and larger oscillations upstream the Manara Bridge.

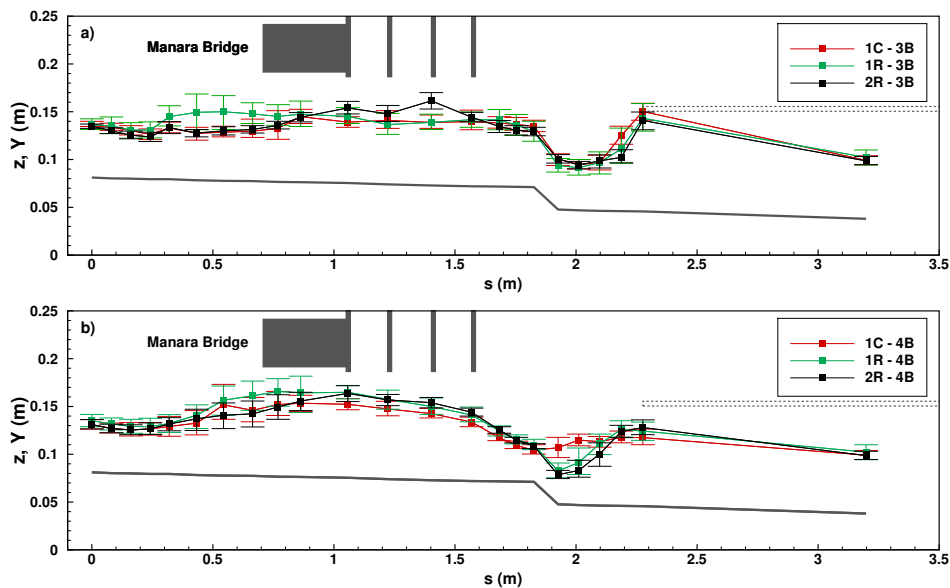


Figure 5. Longitudinal free-surface profiles for experiments *1C*, *1R*, *2R*. Dashed lines indicate ABB car park position. In panel (a), a comparison among the different experiments along the profile 3B; in (b) a comparison among the different experiments along the profile 4B. The profiles 3B and 4B are indicated in Figure 4b.

A second intense hydraulic jump is located downstream the river weir placed downstream of the ELSAG building. This hydraulic jump is less sensitive to the different configurations, since its position is far enough from the confluence where two currents are well mixed. Moreover, also this hydraulic jump is oblique with respect to the longitudinal direction and the reason is the asymmetrical geometry of the weir downstream the ELSAG building.

It is interesting to note that the amplitude of the free surface oscillations, represented by the error bars, tends to decrease moving downstream of the confluence. Moreover, in the configurations *1R*, namely when the Ruscarolo has a greater discharge, the oscillations seem to be larger. The black profiles reported in Figure 5 correspond to the configuration *2R*, where a longitudinal dyke is introduced to damp the transverse free surface oscillations. In particular, the longitudinal dyke was placed in position B, see Figure 3 bottom panel. This orientation has been selected after a comparison with the free surface measurements obtained testing other two dyke orientation, namely A and C. The effect of the dyke is twofold: on one side it effectively damps the free surface oscillations and, on the other side, it modifies the profiles of the mean water depth, inducing a different redistribution of the flow discharges in the three channels downstream the confluence. In Figure 6 the time signals recorded in positions 3B and 4B along the cross section 12, see Figure 4c, for the three positions of the dyke, namely A, B and C, are compared with the configuration *1R*, without the dyke. The water levels recorded in the design configuration show large amplitude oscillations with typical period of few seconds with superimposed high frequency oscillations of small amplitude, the latter are strictly related to the

turbulent flow. It is interesting to show the effect of the dyke on the amplitude of the oscillations and on the water levels inside the culverts. Considering the effect on the free surface oscillations damping, the most effective position is the one labelled A. In fact, the oscillation downstream the Chiaravagna River, on the right bank, is almost completely damped, see Figure 6a,b. At the same time, the mean water level is increased under both culverts. On the contrary, the dyke orientation C, Figure 6e,f, is not effective in damping the oscillations and leaves almost unchanged the mean water level. The position B has been selected based on the relative effectiveness in decreasing the amplitude of the oscillations and, at the same time, without modifying the mean water level. For the latter case, in Table 2 we report an estimate of the free surface oscillation amplitudes. In particular, for each profile reported in Figure 5, we have computed the average and maximum oscillation amplitude as a percentage of the measured flow depth. Note that the mean amplitude of the oscillations for the original design configuration ranges between 10.8% and 16.4% of the mean water depth, reaching maximum values around 30% in the configuration 1R. The effect of the dyke (2R) is to strongly reduce the oscillations for the profile 3B, whereas on the left bank (profile 4B) the damping is less pronounced, i.e., from 14.5% of 1R to 11.1% for 2R.

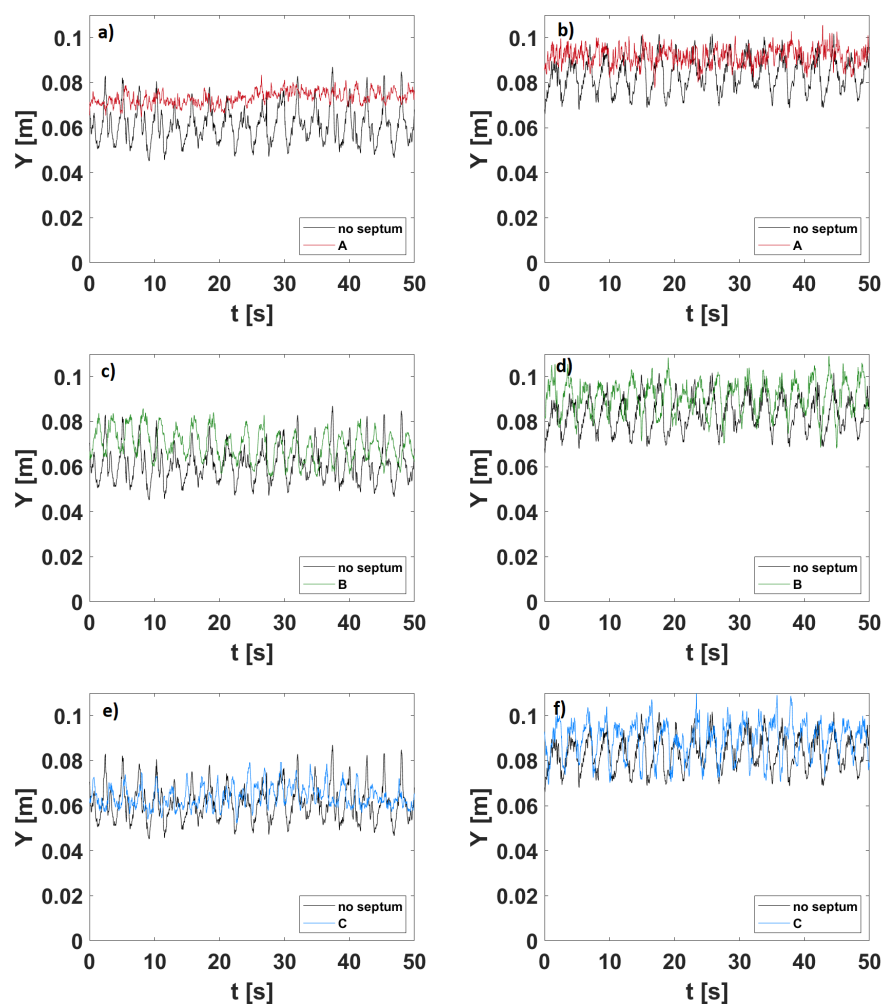


Figure 6. Water level record with different orientations of the longitudinal dyke along the cross section 12, see Figure 4: (a) experiment A water level in position 3B; (b) experiment A water level in position 4B; (c) experiment B water level in position 3B; (d) experiment B water level in position 4B; (e) experiment C water level in position 3B; (f) experiment C water level in position 4B.

Table 2. Comparison among the free surface oscillations amplitude evaluated as a percentage of the water depth for the different configurations.

Configuration	Longitudinal Profile	Maximum Oscillation Amplitude	Mean Oscillation Amplitude
1C	3B	22.6%	10.8%
1R	3B	33.2%	16.4%
2R	3B	13.9%	8.2%
1C	4B	24.1%	11.9%
1R	4B	30.3%	14.5%
2R	4B	24.5%	11.1%

3.2. Time Velocity Distributions

The velocity measurements performed in terms of time signals of the longitudinal ($v_x(x, y, t)$) and transversal component ($v_y(x, y, t)$) are presented in this section. The velocity measurements have been performed in several points along the river reach, see Figure 4a. However, in the present section we show only few typical examples of the velocity records for the sake of brevity.

In Figures 7 and 8, we show the time signals of $v_x(x, y, t)$ and $v_y(x, y, t)$ recorded in two points: one in front of the Chiaravagna River, position 29, and one in front of the Ruscarolo Creek, position 35 of Figure 4a, for the experiments 1R and 2R, respectively. In the same plots the time averaged value of the velocity is represented with a red line.

Figure 7 represents the experiment 1R, with the maximum flow discharge in the Ruscarolo Creek. It can be noticed that the time signals of both components of the velocity show a low frequency oscillation with large amplitude, especially in front of the Ruscarolo Creek. In both positions, the main component of the velocity is the longitudinal one, see Figure 7a,c. Indeed, the mean longitudinal component has values around 0.53–0.75 m/s compared to values around 0.1–0.15 m/s of the mean transversal velocity. The above considerations apply in most of the measuring points in the confluence region for all the experiments performed with the design discharge.

The presence of a circulation zone, which occupies most of the river width, is highlighted by a non negligible transversal velocity component $v_y(x, y, t)$, recorded not only in the position shown but also in several points downstream the confluence between Sections 3 and 8 (see Figure 4b). Movies, recorded during the experiments and attached as Supplementary Materials, help in the visualisation of this recirculating flow region that extends from the left bank to the centre of the confluence. See movies 1 and 2 for the experiments 1C and 1R, respectively.

The positive effect of the presence of the dyke clearly appears also in the velocity signals. Figure 8 shows the velocity signals recorded during experiment 2R, in the same position of the previous run. It is worth noting how the Ruscarolo Creek is not particularly influenced by the presence of the dyke, panel c and d, whereas the flow in front of the Chiaravagna River is remarkably different. Firstly, the peak in the low frequency range disappears and only the high frequency turbulent oscillations are detected. Secondly, the transversal component of the velocity is almost vanished. A transversal velocity is still visible in front of the Ruscarolo Creek where, indeed, a recirculating zone is still present, which is however confined between the left bank and the dyke (see movie 3).

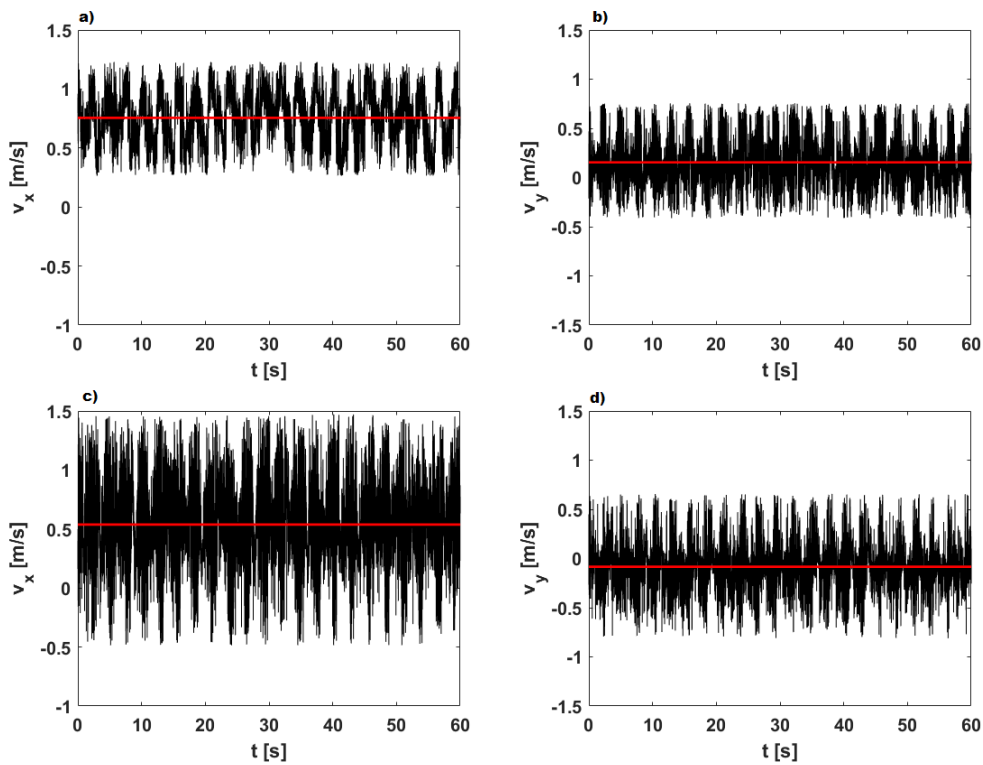


Figure 7. Time signals of the velocity components $v_x(x,y,t)$ and $v_y(x,y,t)$ experiment 1R: (a) $v_x(x,y,t)$ in position 29; (b) $v_y(x,y,t)$ in position 29; (c) $v_x(x,y,t)$ in position 35; (d) $v_y(x,y,t)$ in position 35. The red line represents the mean velocity value.

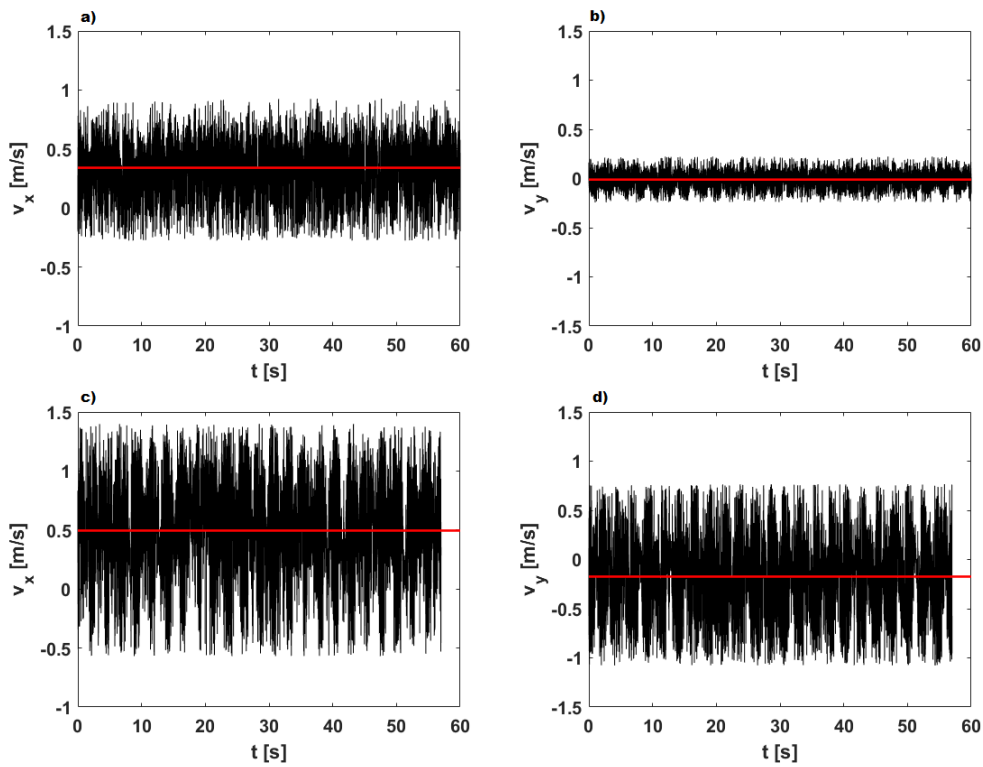


Figure 8. Time signals of the velocity components $v_x(x,y,t)$ and $v_y(x,y,t)$ experiment 2R: (a) $v_x(x,y,t)$ in position 29; (b) $v_y(x,y,t)$ in position 29; (c) $v_x(x,y,t)$ in position 35; (d) $v_y(x,y,t)$ in position 35. The red line represents the mean velocity value.

4. Discussion

The velocity signals show an oscillating character with a clear wide spectrum of frequency. The velocity for the flow under investigation is fully turbulent and, for this reason, the time records of the velocity have been decomposed in a time averaged components plus a fluctuating residual. The velocity residuals have been used to perform a spectral analysis with the aim to describe the characteristic frequency of oscillation of either the free surface instability and the jump toe instability. This approach is very common when the stability of an hydraulic jump is investigated [15–17,25,26].

The spectral analysis is presented on stations 19, 22 and 25, in Figure 4a, which lie along a cross section located in the confluence area.

This helps to identify the variations of the dominant frequencies along the cross section itself. In the following discussion, we intend to show how the free surface fluctuations observed during the experiments, performed with the design discharge, can be rooted to the occurrence of a specific instability of the hydraulic jump, namely the hydraulic jump toe instability. Moreover, we discuss the role of the longitudinal dyke in decreasing the effect of the jump toe instability.

4.1. The Onset of the Free Surface Instability

A dedicated set of experiments on the design configuration, experimental runs from 1 to 23 reported in Table 1, have been performed with the aim of investigating the process that leads to the flow instability already introduced in the previous section.

The critical condition for the onset of the oscillations can be defined based on the spectral analysis of the velocity signals. In fact, the spectral signature of the oscillations should appear quite clearly as a strong peak in the low frequency range, whereas conditions where the flow is undisturbed show a classical scaling of energy spectra for fully three dimensional turbulence.

Figure 9 summarises the stability condition of the whole set of experiments performed, using the total discharge as the main parameter. The different colours of the symbols indicate the experiment showing stable and unstable conditions, in blue and red, respectively. Starting from run 1, the onset of the instability has been observed between flow rates equal to 10.00 and 12.11 l/s. The falling branch has been investigated with differential steps much finer with respect to the rising one, looking for the conditions under which the oscillations naturally were damped. Note that the flow disturbances require a much lower discharge to offset with respect to the critical value for their onset. In fact, the flow returns stable for a discharge equal to 5.83 l/s. This behaviour indicates a possible hysteresis in the response of the system to the flow disturbances. Moreover, this aspect has motivated the rest of the experiments, performed with the aim to detect the critical conditions in more details on a new and finer rising branch. Following the runs from number 10 to 23, the instability has been detected more precisely for the total flow rate between 9.69 and 10.24 l/s, confirming the observations of the first experiments. Note that in previous works only unstable conditions have been investigated, as in [12,15–17,23–25], without looking specifically at the onset of the instability.

In Figure 10, the spatial spectral analysis of the velocity signals are shown for the runs 11, 23 and 18. The velocities have been recorded along a cross section in the confluence area. The y-axis is oriented from Chiaravagna River towards the Ruscarolo Creek.

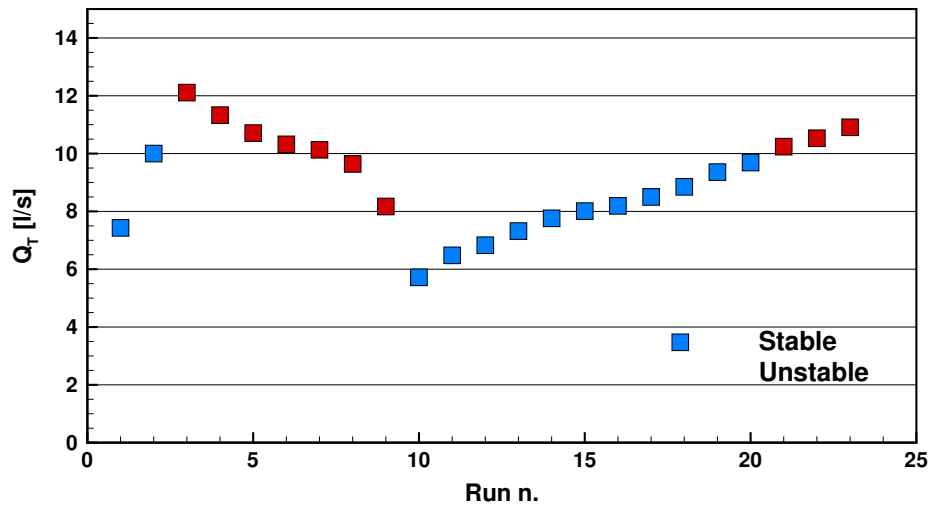


Figure 9. Overview of the experimental conditions as a function of the total discharge: blue dots indicate stable conditions, absence of flow oscillations; red dots give unstable, oscillating flow conditions.

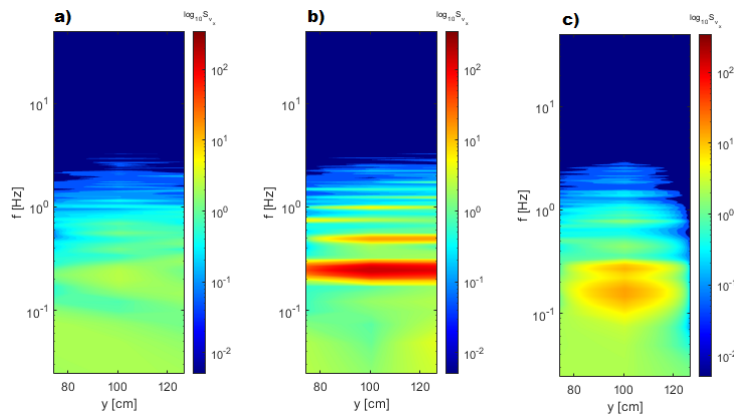


Figure 10. Spectral analysis of the velocity. Panel (a) spatial view of the of the transversal distribution of S_{v_x} run 11; panel (b) spatial view of the of the transversal distribution of S_{v_x} run 23; panel (c) spatial view of the of the transversal distribution of S_{v_x} run 18.

The three experiments selected correspond to flow conditions at which no oscillations occur (run 11), strong velocity fluctuations are clearly detectable (run 23) and, finally, at the onset of the main hydraulic jump toe instability (run 18).

Starting from the stable condition (panel a), the spectrum of the velocity signals displays no particular peaks. In panel b, a fully unstable solution is presented, whereby a clear peak is found for a frequency of about 0.24 HZ, which corresponds to a period of about 4.17 s, and spans the entire cross section. It is worth computing the natural frequency of the system using the dispersion relationship in the limit of shallow water [28], which reads:

$$\omega = \sqrt{gk^2h} \tag{3}$$

where $\omega = 2\pi/T$ is the wave frequency and T the wave period, $k = 2\pi/L$ is the wave-number, L is the wavelength, in this case taken as half of the channel width and h is the local water depth and g the acceleration of gravity. In the specific case of run 23, Equation (3) provides a period of 4.13 s that is fairly close to the frequency detected in the velocity signals. This implies that the jump toe instability, which could be considered as a local instability, is able to trigger the oscillation of the entire domain, since its frequency is equal to the natural frequency of the system.

Finally, considering an experiment close to the critical conditions, e.g., run 18 shown in Figure 10c, a weaker peak is shown limited to the central region of the confluence.

Hydraulic jumps at high Froude numbers are well documented in the literature and free-surface instabilities and jump toe instabilities are often observed, see [12,15–17,23–25]. In the cited works, the jump toe frequencies F_{toe} or its non dimensional form in terms of the Strouhal number $S_t = F_{toe}d_1/V_1$, have been evaluated as a function of the Reynolds number $Re = V_1d_1/\nu$ or as a function of the supercritical upstream Froude number $Fr = d_1/\sqrt{gV_1}$.

In the left panel of Figure 11, the present estimation of S_t as a function of the upstream Froude number of the Ruscarolo Creek is shown together with the measurements of previous studies. The present data are in fairly good agreement with the measurements of previous studies in terms of Strouhal and Froude numbers. Indeed, the Strouhal number seems to be less affected by varying the Froude number as discussed in [15,25]. Note that only Zhang et al. (2013) examined a range of Froude numbers comparable with the present values, whereas all other authors investigated much higher Froude numbers. Moreover, the Strouhal number, estimated in [16], depends on the measurements position, while the present case corresponds to the position closest to the jump toe.

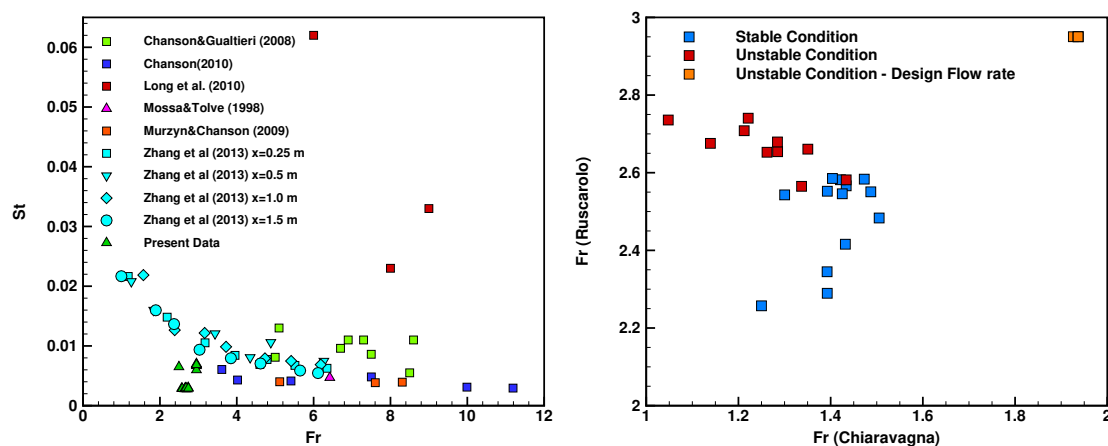


Figure 11. Left panel: Comparison of the present measurements in terms of Strouhal number versus Froude number with previous experiments. Right panel: Froude number of the Ruscarolo creek versus the Froude number of the Chiaravagna river. The stable and unstable conditions are represented by the blue dots and red dots, respectively. In orange the unstable condition for the design flow rates.

The critical conditions for the onset of the hydraulic jump toe instability have also been sought, in terms of critical Froude number. In the right panel of Figure 11, a stability plot is reported as a function of the Froude numbers of the Chiaravagna River and the Ruscarolo Creek, with the same colour coding of Figure 9 except for the orange dots, which represent experimental runs 1C, 1R and 2R. The data are nicely grouped in clusters: the unstable runs are characterised by Froude numbers of the Ruscarolo Creek (the branch with the observed oscillating hydraulic jumps) higher than 2.6, whereas the stable runs occur for Froude numbers of the Ruscarolo below 2.6. Only two runs do not follow this trend (runs 8 and 9) and, not surprisingly, they are both found on the falling branch discussed in Figure 9 with the occurrence of hysteresis process.

Finally, it is worth noting that the design discharge used to test the hydraulic efficiency of the river works, falls in the unstable branch and, in fact, the free surface presents high amplitude frequency that only with the insertion of a longitudinal dyke has been reduced.

4.2. The Effect of the Central Dyke in Damping the Velocity and Free Surface Oscillations

In this section we investigate the influence of the position of the dyke on the flow velocity in terms of oscillation damping. As a general comment, the dyke can influence the dynamics for two main reasons: (I) it represents a rigid longitudinal barrier able to block the transversal flow and damp

the oscillations; (II) it segregates the hydraulic jump instability in a region downstream the Ruscarolo reach close to the left bank.

With the aim to understand the effect of changing the position of the dyke (see Figure 3 bottom panel), we performed specific measurements of the velocity along the same cross section used before in the analysis of the frequency of the hydraulic jump instability.

Figure 12 reports the comparison between the PSDs calculated in absence of the dyke (panel d) and in the three configurations A, B and C (panels a,b and c, respectively). The effect of the position of the dyke appears quite clearly, comparing panel d (no dyke) with the other panels: with the dyke in position A, peaks in PSDs are detectable both in the Chiaravagna and the Ruscarolo reaches. Moving to position B (panel b), the peaks in the velocity spectrum are strongly reduced in both branches. Position C (panel c) produces a stronger confinement of the disturbances: a less intense peak is still detectable only in front of the Ruscarolo reach.

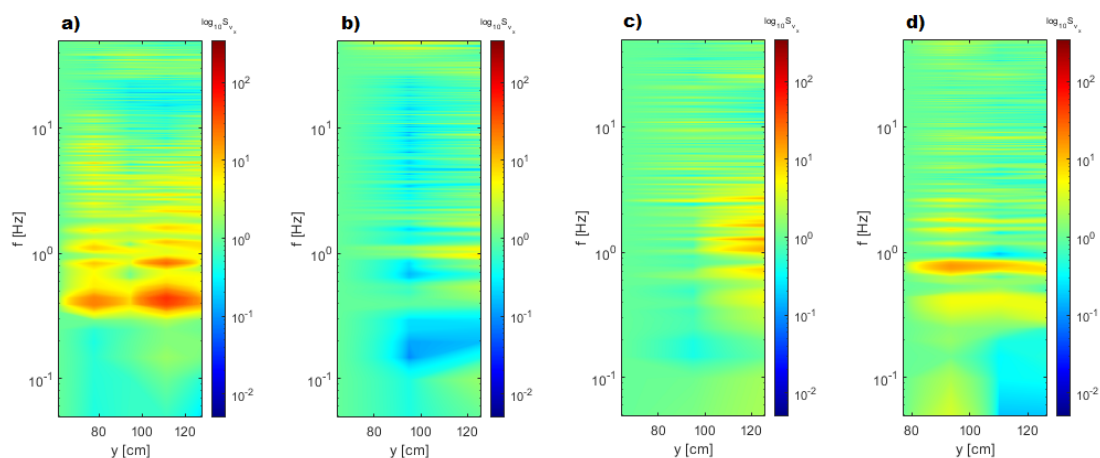


Figure 12. Spatial spectral analysis of the velocity signal recorded at cross section 5 of Figure 4c. Experimental condition R: panel (a) dyke in position A; panel (b) dyke in position B; panel (c) dyke in position C; panel (d) no dyke (run 1R).

5. Conclusions

In this study we have experimentally investigated the hydraulic response of a real river confluence using a scaled physical model of the part of the Chiaravagna River and Ruscarolo Creek including a short undisturbed reach and a long reach after their confluence. To increase the flow capacity of the reach, upstream and downstream the river confluence, river works have been recently designed. The main purpose of the experiments was to test the effectiveness of the design solution. The river confluence has been tested for a flood event with return period equal to 200 years, and the experiments showed the occurrence of intense transversal free surface oscillations, which might dramatically increase the flooding risk. In fact, the amplitude of the oscillations was estimated to be up to 30% of the mean water level. The measurements have demonstrated that the transversal oscillations are triggered by the instability of the toe of the oblique hydraulic jumps of the Ruscarolo Creek in correspondence of the confluence. The typical jump toe instability frequency has been found to be close to the free mode of oscillation of the channel at the confluence. Thus, the jump toe instability is able to excite the transversal mode of instability of the entire channel. The measured non dimensional toe frequency, i.e., the Strouhal number, as a function of the super-critical Froude number have been found in good agreement with published studies. Moreover, the critical conditions have been analysed with the aim to find the critical Froude number for the onset of the hydraulic jump toe instability. The critical Froude number has been found to be around a value of 2.6. Finally, the possibility to add to the original project a longitudinal dyke placed within the river confluence has been investigated. The dyke has been found

to be effective in the oscillation damping, confining the instability in a smaller portion of the cross section, namely on the left bank downstream the Ruscarolo Creek.

The results suggest that hydraulic jump instability might play an important role in realistic conditions of river confluence, especially for river reaches in supercritical conditions. This situation is not uncommon in several small basins with relatively high bed slopes. Thus, considering this unsteady phenomena might be important when flood defence river works are planned.

Supplementary Materials: The following are available online at <http://www.mdpi.com/2073-4441/12/7/2027/s1>, Figure S1: View of the model confluence from upstream on the Chiaravagna River side, Figure S2: Detail of the model confluence, from right bank, Figure S3: View of the complete model from downstream, Figure S4: Detail of the ELSAG pillars and Via Manara Bridge, view from the left bank, Figure S5: Detail of the ELSAG pillars and Via Manara Bridge, view from downstream, Figure S6: View of the Ruscarolo Creek and Old Arch Bridge from downstream, Figure S7: Detail of the ELSAG pillars and pedestrian bridge, view from downstream: Chiaravagna River is on the left side of the figure, whereas Ruscarolo Creek is on the right, Figure S8: View of the Chiaravagna River from downstream, Figure S9: Detail of the dyke in position B and Ruscarolo weir, Figure S10: View from downstream of the ABB car park, Figure S11: Detail of the model confluence with dyke in position B, view from right bank.

Author Contributions: All authors contributed to the building of this paper in its different aspects. Conceptualisation: M.C. and A.S.; experiments: A.D.L., A.R. and A.S.; data analysis: A.D.L., A.R., M.P., M.C. and A.S. writing—original draft preparation: A.D.L., M.P., M.C. and A.S.; writing—review and editing: A.D.L., A.R., M.P., M.C. and A.S. All authors have read and agreed to the published version of the manuscript.

Acknowledgments: The study has been financially supported by ITEC Engineering, responsible for the river works design. We thank Ing. Pinasco of the Comune di Genova, public Authority in charge of the flood risk management of the City of Genova (Italy) and Prof. Maurizio Brocchini for the fruitful discussion on the experimental measurements.

Conflicts of Interest: The authors declare no conflict of interest.

Abbreviations

The following abbreviations are used in this manuscript:

PSD	Power Spectral Density
F_r	Froude number
S_t	Strouhal number

References

1. Hager, W.H. *Energy Dissipators and Hydraulic Jump*; Springer Science & Business Media: Berlin, Germany, 2013; Volume 8.
2. Endreny, T.; Lautz, L.; Siegel, D. Hyporheic flow path response to hydraulic jumps at river steps: Flume and hydrodynamic models. *Water Resour. Res.* **2011**, *47*.
3. Wildhaber, Y.S.; Michel, C.; Epting, J.; Wildhaber, R.; Huber, E.; Huggenberger, P.; Burkhardt-Holm, P.; Alewell, C. Effects of river morphology, hydraulic gradients, and sediment deposition on water exchange and oxygen dynamics in salmonid redds. *Sci. Total Environ.* **2014**, *470*, 488–500.
4. Grant, S.B.; Gomez-Velez, J.D.; Ghisalberti, M. Modeling the effects of turbulence on hyporheic exchange and local-to-global nutrient processing in streams. *Water Resour. Res.* **2018**, *54*, 5883–5889.
5. Bakhmeteff, B.A. The hydraulic jump in terms of dynamic similarity. *Trans. Am. Soc. Civ. Eng. ASCE* **1936**, *61*, 145–162.
6. Rouse, H.; Siao, T.T.; Nagaratnam, S. Turbulence characteristics of the hydraulic jump. *J. Hydraul. Div.* **1958**, *84*, 1–30.
7. Bélanger, J. *Notes sur l'Hydraulique*; Ecole Royale des Ponts et Chaussées: Paris, France, 1841; Volume 1842, p. 223.
8. Henderson, F.M. *Open Channel Flow*; Macmillan Co., Inc.: New York, NY, USA, 1966.
9. Chanson, H. Development of the Bélanger equation and backwater equation by Jean-Baptiste Bélanger (1828). *J. Hydraul. Eng.* **2009**, *135*, 159–163.
10. Chanson, H. Momentum considerations in hydraulic jumps and bores. *J. Irrig. Drain. Eng.* **2012**, *138*, 382–385.
11. Lennon, J.; Hill, D. Particle image velocity measurements of undular and hydraulic jumps. *J. Hydraul. Eng.* **2006**, *132*, 1283–1294.

12. Long, D.; Rajaratnam, N.; Steffler, P.M.; Smy, P.R. Structure of flow in hydraulic jumps. *J. Hydraul. Res.* **1991**, *29*, 207–218.
13. Hager, W.H.; Bretz, N.V. Hydraulic jumps at positive and negative steps. *J. Hydraul. Res.* **1986**, *24*, 237–253.
14. Chanson, H.; Brattberg, T. Experimental study of the air–water shear flow in a hydraulic jump. *Int. J. Multiph. Flow* **2000**, *26*, 583–607.
15. Chanson, H. Convective transport of air bubbles in strong hydraulic jumps. *Int. J. Multiph. Flow* **2010**, *36*, 798–814.
16. Zhang, G.; Wang, H.; Chanson, H. Turbulence and aeration in hydraulic jumps: Free-surface fluctuation and integral turbulent scale measurements. *Environ. Fluid Mech.* **2013**, *13*, 189–204.
17. Wang, H.; Chanson, H. Experimental study of turbulent fluctuations in hydraulic jumps. *J. Hydraul. Eng.* **2015**, *141*, 04015010.
18. Montano, L.; Felder, S. An experimental study of air–water flows in hydraulic jumps on flat slopes. *J. Hydraul. Res.* **2019**, 1–11.
19. Valero, D.; Viti, N.; Gualtieri, C. Numerical Simulation of Hydraulic Jumps. Part 1: Experimental Data for Modelling Performance Assessment. *Water* **2019**, *11*, 36.
20. Viti, N.; Valero, D.; Gualtieri, C. Numerical simulation of hydraulic jumps. Part 2: Recent results and future outlook. *Water* **2019**, *11*, 28.
21. Jesudhas, V.; Balachandar, R.; Bolisetti, T. Numerical study of a symmetric submerged spatial hydraulic jump. *J. Hydraul. Res.* **2019**, 1–15.
22. Jesudhas, V.; Balachandar, R.; Wang, H.; Murzyn, F. Modelling hydraulic jumps: IDDES versus experiments. *Environ. Fluid Mech.* **2020**, 1–21.
23. Mossa, M. On the oscillating characteristics of hydraulic jumps. *J. Hydraul. Res.* **1999**, *37*, 541–558.
24. Mossa, M.; Tolve, U. Flow Visualization in Bubbly Two-Phase Hydraulic Jump. *Trans. ASME* **1998**.
25. Murzyn, F.; Chanson, H. Free-surface fluctuations in hydraulic jumps: Experimental observations. *Exp. Therm. Fluid Sci.* **2009**, *33*, 1055–1064.
26. Kramer, M.; Valero, D. Turbulence and self-similarity in highly aerated shear flows: The stable hydraulic jump. *Int. J. Multiph. Flow* **2020**, 103316.
27. Chanson, H.; Gualtieri, C. Similitude and scale effects of air entrainment in hydraulic jumps. *J. Hydraul. Res.* **2008**, *46*, 35–44.
28. Pedlosky, J. *Geophysical Fluid Dynamics*; Springer Science & Business Media: Berlin, Germany, 2013.



© 2020 by the authors. Licensee MDPI, Basel, Switzerland. This article is an open access article distributed under the terms and conditions of the Creative Commons Attribution (CC BY) license (<http://creativecommons.org/licenses/by/4.0/>).